NASA TECHNICAL NOTE

NASA TN D-3894

NASA TN D-3894

HYPERSONIC PERFORMANCE OF SEVERAL BASIC AND MODIFIED DIAMOND-CROSS-SECTION DELTA-WING CONFIGURATIONS

by Leonard M. Weinstein and Luther Neal, Jr.

Langley Research Center
Langley Station, Hampton, Va.

NATIONAL AERONAUTICS AND SPACE ADMINISTRATION • WASHINGTON, D. C. • APRIL 1967

NASA TN D-3894

HYPERSONIC PERFORMANCE OF SEVERAL BASIC AND MODIFIED DIAMOND-CROSS-SECTION DELTA-WING CONFIGURATIONS

By Leonard M. Weinstein and Luther Neal, Jr.

Langley Research Center
Langley Station, Hampton, Va.

NATIONAL AERONAUTICS AND SPACE ADMINISTRATION

For sale by the Clearinghouse for Federal Scientific and Technical Information
Springfield, Virginia 22151 – CFSTI price $3.00

HYPERSONIC PERFORMANCE OF SEVERAL BASIC AND MODIFIED DIAMOND-CROSS-SECTION DELTA-WING CONFIGURATIONS

By Leonard M. Weinstein and Luther Neal, Jr.
Langley Research Center

SUMMARY

An investigation of the hypersonic performance of several delta wings with diamond cross sections was conducted in the Langley 11-inch hypersonic tunnel, and the effects of modifications to some of these wings were determined. The modifications were made in order to remove regions of high drag and to make the configurations more compact. The unmodified models had leading-edge sweep angles ranging from 60° to 82° and ratios of base thickness to root chord from about 0.06 to 0.21. These models were tested at free-stream Mach numbers of 6.8 and 9.7 over a range of free-stream Reynolds numbers based on root chord from 0.3×10^6 to 3.2×10^6. The effects of the various modifications (removal of parts of the top, bottom, and tips) were studied at a Mach number of 6.8 and a free-stream Reynolds number based on root chord of 1.4×10^6.

The results showed that for the unmodified models the maximum lift-drag ratio increased with increasing free-stream Reynolds number based on root chord, but the increase was less than the amount indicated by laminar theory, which included the effects of viscous interaction. The lesser increase was probably due to the onset of transitional flow. For the same Reynolds number, the values of maximum lift-drag ratio were lower at Mach 9.7 than at Mach 6.8 by an amount roughly equal to that predicted by theory. All modifications increased the maximum lift-drag ratio, as predicted by theory; however, the magnitudes of maximum lift-drag ratio were 10 to 15 percent lower than the theoretical values. The major geometric correlating parameter for maximum lift-drag ratio was found to be an effective thickness ratio defined as the mean local thickness ratio.

INTRODUCTION

Cruise vehicles at hypersonic speeds and lifting reentry vehicles require high lift-drag ratios for efficient long-range flight within the earth's atmosphere. As part of a general program establishing design guidelines for hypersonic vehicles with high lift-drag ratios, investigations of various configuration shapes are underway. Some of the recent results obtained from this program are presented in references 1 to 6 for several different basic shapes. For example, wing-body and lifting body configurations are

considered in references 1 to 4, and reference 5 pertains to delta wings with triangular cross sections and to rectangular-wedge wings. In reference 6, a study of the effects of geometric modifications on the maximum lift-drag ratios of slender wing bodies is presented.

The purpose of the present study is to investigate the hypersonic performance of several delta wings with diamond cross sections and to determine the effects of successive geometric modifications on the performance of these wings. The modifications are made in order to remove regions of high drag and to make the configurations more compact.

SYMBOLS

b	width of model base, centimeters
$\bar{c}$	mean aerodynamic chord, centimeters
C_A	axial-force coefficient, $\frac{\text{Axial force}}{q_\infty S}$
C_D	drag coefficient, $\frac{\text{Drag}}{q_\infty S}$
$C_{D,o}$	drag coefficient at $\alpha = 0^o$
$C_{D,ip}$	inviscid-pressure drag coefficient
$(C_{D,p})_d$	pressure drag coefficient due to boundary-layer displacement effects
C_F	average laminar skin-friction drag coefficient including boundary-layer displacement effects
C_m	pitching-moment coefficient, $\frac{\text{Pitching moment}}{q_\infty S\bar{c}}$
C_N	normal-force coefficient, $\frac{\text{Normal force}}{q_\infty S}$
c_r	root chord, centimeters
L/D	lift-drag ratio
$(L/D)_{max}$	maximum lift-drag ratio

M_l	local Mach number
M_∞	free-stream Mach number
q_∞	free-stream dynamic pressure
R_{l,c_r}	local Reynolds number based on root chord
R_{∞,c_r}	free-stream Reynolds number based on root chord
S	planform area, centimeter^2
t	thickness at model base, centimeters
t_{eff}	effective thickness of model that corresponds to the mean model wedge angle, centimeters
V	volume of model, centimeter^3
x	distance from nose of model to moment reference (at $0.5\bar{c}$), centimeters
α	angle of attack, angle between center line of unmodified model and free-stream flow direction
α_{opt}	angle of attack at which $(L/D)_{max}$ occurs
Λ	wing sweep angle
θ	maximum half-wedge angle (between ridge line and center line of unmodified model)
ϕ	ratio of local thickness of model to distance from leading edge measured along local chord

APPARATUS AND TESTS

Models

Sketches of the configurations along with tabulated geometric properties of the models are presented in figure 1. Configuration A, the basic configuration, consists of a

sharp-edged delta wing with diamond cross section. The unmodified models had leading-edge sweep angles from 60° to 82° and ratios of base thickness to root chord from about 0.06 to 0.21. Configurations B, C, D, and E are modifications of configuration A, as described in the following table:

Modified configuration	Nature of modification to configuration A
Configuration B	25 percent of base height was removed by a horizontal plane parallel to model center line
Configuration C	50 percent of base height was removed by a horizontal plane to produce a half model
Configuration D	25 percent of base height was removed from both the top and the bottom by horizontal planes parallel to model center line
Configuration E	25 percent of base height was removed from both the top and the bottom (as for configuration D), and the model tips were removed by vertical planes parallel to the model center line so as to produce the same value of $V^{2/3}/S$ as for configuration A

The effects of each type of modification were investigated for a sizable range of sweep angles and ratios of base thickness to root chord. Configuration B and configuration C models were tested both in the position shown in figure 1 (flat-top orientation) and in the inverted position (flat-bottom orientation). All models were constructed of stainless steel and had swept leading edges that were from 0.003 centimeter to 0.007 centimeter thick.

Tunnel and Nozzles

The investigation was conducted in the Langley 11-inch hypersonic tunnel. This facility utilizes different fixed-geometry nozzles to facilitate testing at different Mach numbers. For the present investigation the Mach 6.8 and Mach 9.7 air nozzles were employed. The Mach 6.8 nozzle is a two-dimensional contoured nozzle constructed of invar to minimize distortion of the throat section due to aerodynamic heating, whereas the Mach 9.7 nozzle is a contoured three-dimensional nozzle. The free-stream Mach number of both nozzles varies with free-stream Reynolds number because of corresponding changes in tunnel-wall boundary-layer thickness. For a range of stagnation pressures from 5 to 40 atmospheres, the test-section Mach number when the Mach 6.8 nozzle is used varies from about 6.7 to 6.9. For the range of usable stagnation

pressures from 15 to 45 atmospheres, the test-section Mach number when the Mach 9.7 nozzle is used varies from about 9.6 to 9.75. When the Mach 6.8 nozzle is used, the test-section Mach number is also dependent on time, but to a lesser extent than on stagnation pressure. The time dependence is due to a slight distortion of the throat section caused by thermal gradients. For a 60-second run at a given stagnation pressure, the Mach number varies by about 0.05. Typical calibrations of the nozzles may be found in reference 7, and a further description of the test facility is given in reference 8.

Test Conditions and Procedures

The main part of the investigation was conducted at Mach 6.8. At this Mach number the basic wings (configuration A models) were tested at stagnation pressures ranging from 5 to 35 atmospheres with an average stagnation temperature of 620° K. These conditions resulted in a range of free-stream Reynolds numbers based on root chord from 0.264×10^6 to 3.11×10^6.

In order to study Mach number effects, some of the basic models were also tested at a Mach number of 9.7. The investigation at Mach 9.7 was conducted at a stagnation temperature of 950° K and at stagnation pressures of 33 and 44 atmospheres with corresponding free-stream Reynolds numbers based on root chord from 0.308×10^6 to 0.751×10^6.

The stagnation temperatures quoted were sufficient to prevent liquefaction of air in the test section. Water condensation effects were avoided by keeping the absolute humidity of the air sufficiently low.

A three-component strain-gage balance was used to obtain the force and moment data over a range of angles of attack from -2° to 10°. Two methods were used to determine the angle of attack. For some of the models, a small prism mounted on the base of the model reflected a beam of light onto a calibrated scale. This method gives the true angle of attack regardless of deflection of the balance and sting under load. For the other models (generally the thinner ones), the angle of attack was set from a no-load indicator and schlieren photographs were used to measure the actual angle of attack under load conditions.

In reducing the experimental data, account was taken of the previously noted variation of free-stream Mach number with both time and stagnation pressure. The axial-force data were adjusted to correspond to the condition of free-stream pressure over the base of the model.

Accuracy of Data

Stagnation pressure was read from a Bourdon gage to an accuracy of about ±0.06 atmosphere. The angles of attack are estimated to have an accuracy of $\pm 0.2^{o}$. The Mach number is known to be about ±0.03. The force balance system gives repeatability within about ±0.5 percent full load. Errors from these sources plus probable errors due to the inaccuracy of base-pressure measurements resulted in the following typical uncertainties in the aerodynamic coefficients:

ΔC_N	±0.002
ΔC_A	±0.001
ΔC_m	±0.001
$\Delta (L/D)_{max}$	±0.3

RESULTS AND DISCUSSION

Summary plots of the data are presented in figures 2 to 6. Schlieren photographs are shown in figure 7 for three modified wings at fairly high angles of attack. Basic aerodynamic data for a Mach number of 6.8 and a free-stream Reynolds number based on root chord of 1.4×10^6 are given in figure 8.

Reynolds Number Effects on $C_{D,o}$

Since skin-friction and pressure effects are comparable in magnitude for slender wings at the test conditions, a knowledge of the type of boundary layer present is important in analyzing the experimental results. In figure 2, the variation of $C_{D,o}$ with R_{∞,c_r} is shown for three of the basic models at $M_\infty = 6.8$. Included with the data are results from laminar theory. The total curves for $C_{D,o}$ were obtained from addition of C_F, $(C_{D,p})_d$, and $C_{D,ip}$. These coefficients were obtained by the method of reference 9, which takes into account the displacement effects of the boundary layer. In using the method of reference 9, the geometric angle of attack of each panel was taken as the minimum angle between the free-stream velocity vector and the panel. The data show a departure from the laminar-theory curves at the higher Reynolds numbers. Thus, transition on slender wings and wing bodies would occur at rather low local Reynolds numbers based on length from leading edge measured parallel to ridge line (on the order of 0.5×10^6) compared with the usual transition Reynolds numbers of a two-dimensional flat plate (ref. 10). Nevertheless, since the data for most models in the present study follow the laminar theory fairly closely up to a value of R_{∞,c_r} of about 1.4×10^6, this nominal Reynolds number was selected as the one at which to study the effects of the modifications to the basic shapes.

Mach Number and Reynolds Number Effects on $(L/D)_{max}$

The available data showing the effects of M_∞ and R_{∞,c_r} on $(L/D)_{max}$ are presented in figure 3. It should be noted that, for model 1-A at $R_{\infty,c_r} = 1.4 \times 10^6$, the angle-of-attack range did not reach α_{opt} so $(L/D)_{max}$ was found by extrapolating the results obtained at the lower Reynolds numbers. In order to avoid confusion, laminar-theory curves are shown only for the models with the two extremes in thickness ratio (models 1-A and 6-A). Theory for models with other thickness ratios gave comparable results. The Mach 6.8 data are seen to increase with increasing Reynolds number much more slowly than indicated by theory and, in fact, to level off at the higher Reynolds numbers while the laminar-theory curves are still rapidly increasing. The probable reason is the onset of transitional flow. The values of $(L/D)_{max}$ at Mach 9.7 are lower than corresponding values at Mach 6.8 by an amount roughly equal to that predicted by theory.

It is interesting to note that model 3-A at Mach 6.8 and model 5-A at Mach 9.7 show the same level of $(L/D)_{max}$. Likewise, the level of $(L/D)_{max}$ for model 1-A at Mach 6.8 and model 2-A at Mach 9.7 is the same. Both pairs of models are hypersonically similar $\left(\text{i.e., the models in each pair have the same value of } M_\infty \frac{t}{c_r} \text{ and of } M_\infty \frac{b}{c_r}\right)$.

Effects of Wing Modifications

The effects of wing modifications are illustrated in figure 4 where the experimental values of $(L/D)_{max}$ are plotted as functions of the volumetric efficiency parameter $V^{2/3}/S$. For a particular model, the effects of modifications are found by following the arrows and noting that the symbol shape represents the cross section of the base. All the modifications result in improvements in $(L/D)_{max}$ but, except for configuration E models, in decreases in $V^{2/3}/S$. The data for all models, plotted in the lower right-hand corner of figure 4, indicate roughly the amount of improvement in $(L/D)_{max}$ and also show the general trend – that is, a decrease in $V^{2/3}/S$ results in an increase in $(L/D)_{max}$. Also, the flat-bottom models generally exhibit slightly higher maximum lift-drag ratios than the flat-top models, as had been observed in reference 5.

Figure 5 shows a comparison between laminar theory and experimental data for $(L/D)_{max}$ for the major modifications to model 5. It is seen that, at $R_{\infty,c_r} = 1.4 \times 10^6$, theory predicts well the trend of the changes in $(L/D)_{max}$ with the modifications; however, the data are consistently overpredicted by about 10 to 15 percent. These results are representative of those obtained with other models.

The apparent scatter of the data that was observed in the lower right-hand corner of figure 4 is, of course, due to the fact that $(L/D)_{max}$ is not a simple function of $V^{2/3}/S$. However, theoretical calculations for the basic slender delta wings show that, if the thickness ratio is held constant, $(L/D)_{max}$ remains relatively unchanged with changes in other geometric parameters (see also ref. 5). This result suggests that for slender wings having more complex shapes there could be an effective thickness ratio which would correlate $(L/D)_{max}$. In figure 6, $(L/D)_{max}$ is plotted as a function of an effective thickness ratio which is defined as the mean local thickness ratio – that is,

$$\frac{t_{eff}}{c_r} = \frac{1}{\int_S dS} \int_S \phi \, dS$$

In general, the data correlate well and follow the trend shown by the theory.

Schlieren Photographs

Schlieren photographs are shown in figure 7 for three representative models at fairly high angles of attack. The model shown in figure 7(a) has a fairly thick attached boundary layer on the leeward side. Figure 7(b) shows a model with a boundary layer that may be separated on the leeward surface. An illustration of a model with a very thick viscous layer on the rearward portion of the leeward side is presented in figure 7(c). Thick viscous layers on the leeward surface of some models may be a factor contributing to the disagreement between experimental and theoretical values of $(L/D)_{max}$.

CONCLUDING REMARKS

An investigation of the hypersonic performance of several delta wings with diamond cross sections was conducted in the Langley 11-inch hypersonic tunnel, and the effects of modifications to some of these wings were determined. For the basic models at Mach 6.8, a comparison of laminar-theory curves with experimental data indicates that transitional flow occurred at moderately low local Reynolds numbers, based on length from leading edge measured parallel to ridge line, compared with the usual flat-plate transition Reynolds numbers. At a free-stream Reynolds number based on root chord of 1.4×10^6, where the flow was believed to have been predominately laminar over the models, the values of maximum lift-drag ratio were overpredicted by theory for all configurations by about 10 to 15 percent. The values of maximum lift-drag ratio for the basic models at Mach 9.7 were lower than corresponding values at Mach 6.8 by an amount roughly equal to that predicted by theory. Modifying the wing by removing portions of

the top or bottom improved the maximum lift-drag ratio but caused a corresponding decrease in the volumetric efficiency parameter. Subsequent removal of the tips of the wings returned the volumetric efficiency parameter to the initial value, while the improvement in $(L/D)_{max}$ was maintained. The major geometric correlating parameter for maximum lift-drag ratio was found to be an effective thickness ratio defined as the mean local thickness ratio.

Langley Research Center,
National Aeronautics and Space Administration,
Langley Station, Hampton, Va., November 21, 1966,
129-01-09-03-23.

REFERENCES

1. Fetterman, David E.: Favorable Interference Effects on Maximum Lift-Drag Ratios of Half-Cone Delta-Wing Configurations at Mach 6.86. NASA TN D-2942, 1965.

2. Johnston, Patrick J.; Snyder, Curtis D.; and Witcofski, Robert D.: Maximum Lift-Drag Ratios of Delta-Wing—Half-Cone Combinations at a Mach Number of 20 in Helium. NASA TN D-2762, 1965.

3. Fetterman, David E.; Henderson, Arthur, Jr.; Bertram, Mitchel H.; and Johnston, Patrick J.: Studies Relating to the Attainment of High Lift-Drag Ratios at Hypersonic Speeds. NASA TN D-2956, 1965.

4. Becker, John V.: Studies of High Lift/Drag Ratio Hypersonic Configurations. Proceedings of the 4th Congress of the International Council of the Aeronautical Sciences, Robert R. Dexter, ed., Spartan Books, Inc., 1965, pp. 877-910.

5. Penland, Jim A.: Maximum Lift-Drag-Ratio Characteristics of Rectangular and Delta Wings at Mach 6.9. NASA TN D-2925, 1965.

6. Small, William J.; and Bertram, Mitchel H.: Effect of Geometric Modifications on the Maximum Lift-Drag Ratios of Slender Wing-Body Configurations at Hypersonic Speeds. NASA TN D-3276, 1966.

7. Bertram, Mitchel H.: Boundary-Layer Displacement Effects in Air at Mach Numbers of 6.8 and 9.6. NASA TR R-22, 1959. (Supersedes NACA TN 4133.)

8. McLellan, Charles H.; Williams, Thomas W.; and Beckwith, Ivan E.: Investigation of the Flow Through a Single-Stage Two-Dimensional Nozzle in the Langley 11-Inch Hypersonic Tunnel. NACA TN 2223, 1950.

9. Bertram, Mitchel H.: Hypersonic Laminar Viscous Interaction Effects on the Aerodynamics of Two-Dimensional Wedge and Triangular Planform Wings. NASA TN D-3523, 1966.

10. Bertram, Mitchel H.: Exploratory Investigation of Boundary-Layer Transition on a Hollow Cylinder at a Mach Number of 6.9. NACA Rept. 1313, 1957. (Supersedes NACA TN 3546.)

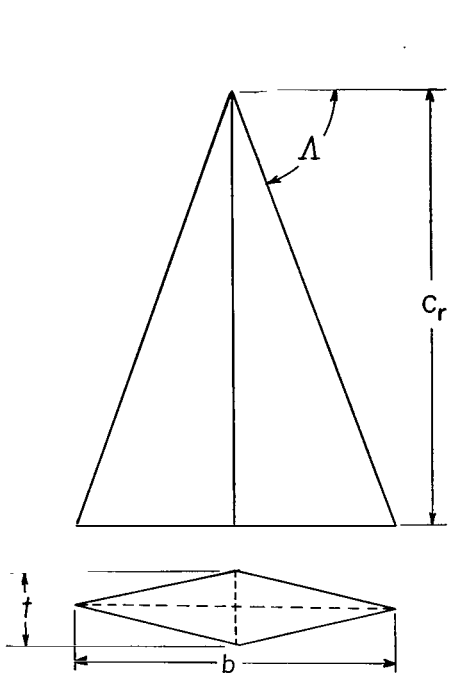

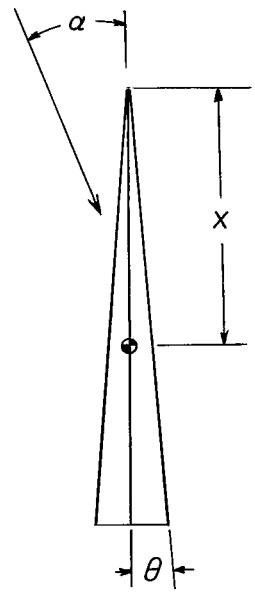

Configurations

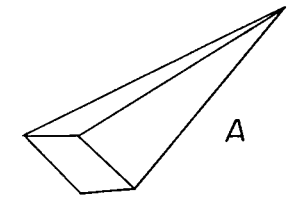

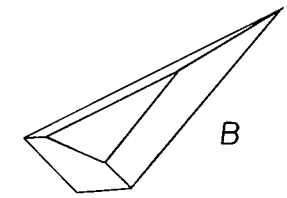

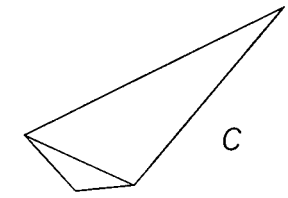

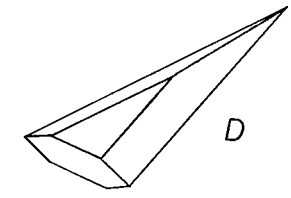

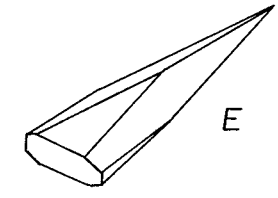

Model	c_r, cm	t, cm	Λ, deg	θ, deg	$V^{2/3}/S$	S, cm^2	x, cm	b, cm
1-A	11.00	2.31	60	6	0.204	69.8	7.34	12.70
1-B	↓	1.73	↓	↓	.195	↓	↓	↓
1-C	↓	1.16	↓	↓	.128	↓	↓	↓
2-A	16.19	2.44	68.57	4.32	.186	102.9	10.80	12.70
2-D	↓	1.22	↓	↓	.170	↓	↓	↓
2-E	↓	↓	↓	↓	.186	91.6	10.34	8.51
3-A	15.25	2.60	70	4.89	.207	84.5	10.16	11.11
3-D	↓	1.30	↓	↓	.190	↓	↓	↓
3-E	↓	↓	↓	↓	.207	75.3	9.74	7.42
4-A	17.85	2.43	70.4	3.92	.180	113.2	11.90	12.70
4-B	↓	1.82	↓	↓	.172	↓	↓	↓
4-C	↓	1.22	↓	↓	.113	↓	↓	↓
4-D	↓	↓	↓	↓	.165	↓	↓	↓
5-A	20.31	2.48	75.71	3.50	.187	104.9	13.55	10.35
5-B	↓	1.86	↓	↓	.179	↓	↓	↓
5-C	↓	1.31	75	3.69	.120	110.5	↓	10.88
5-D	↓	1.24	75.71	3.50	.171	104.9	↓	10.37
5-E	↓	↓	↓	↓	.187	93.4	13.00	6.93
6-A	22.22	1.40	82.38	1.86	.148	66.0	14.82	5.94
7-A	20.31	1.63	78.57	2.30	.153	83.4	13.55	8.20

Figure 1.- Sketch of configurations and table of model dimensions.

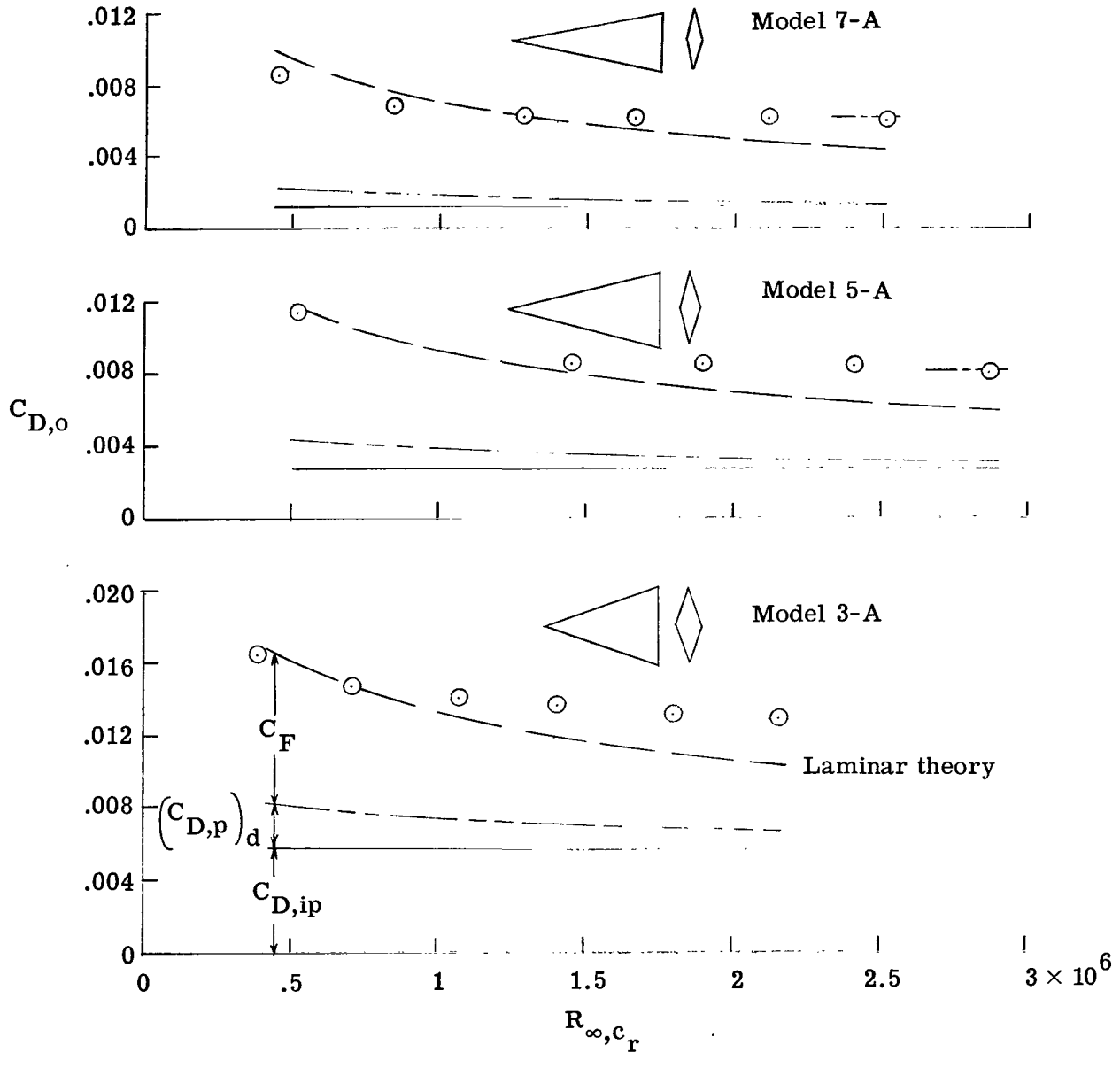

Figure 2.- Effects of free-stream Reynolds number based on root chord on the drag coefficient at $\alpha = 0^0$ for three basic models. $M_\infty = 6.8$; $M_l/M_\infty = 0.88$ to 0.94; $\frac{R_{l,c_r}}{R_{\infty,c_r}} = 1.1$ to 1.3.

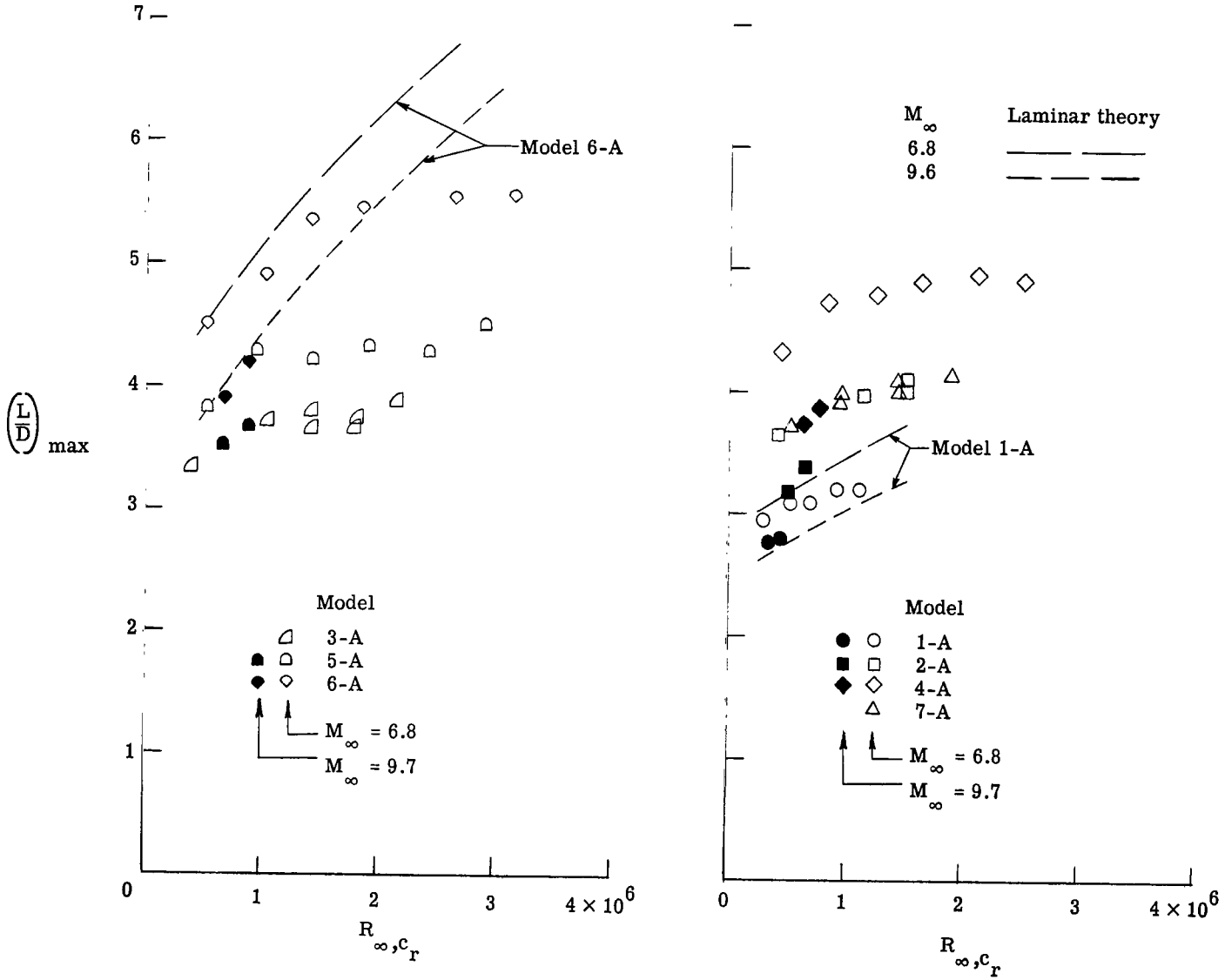

Figure 3.- Effects of free-stream Mach number and free-stream Reynolds number based on root chord on $(L/D)_{max}$.

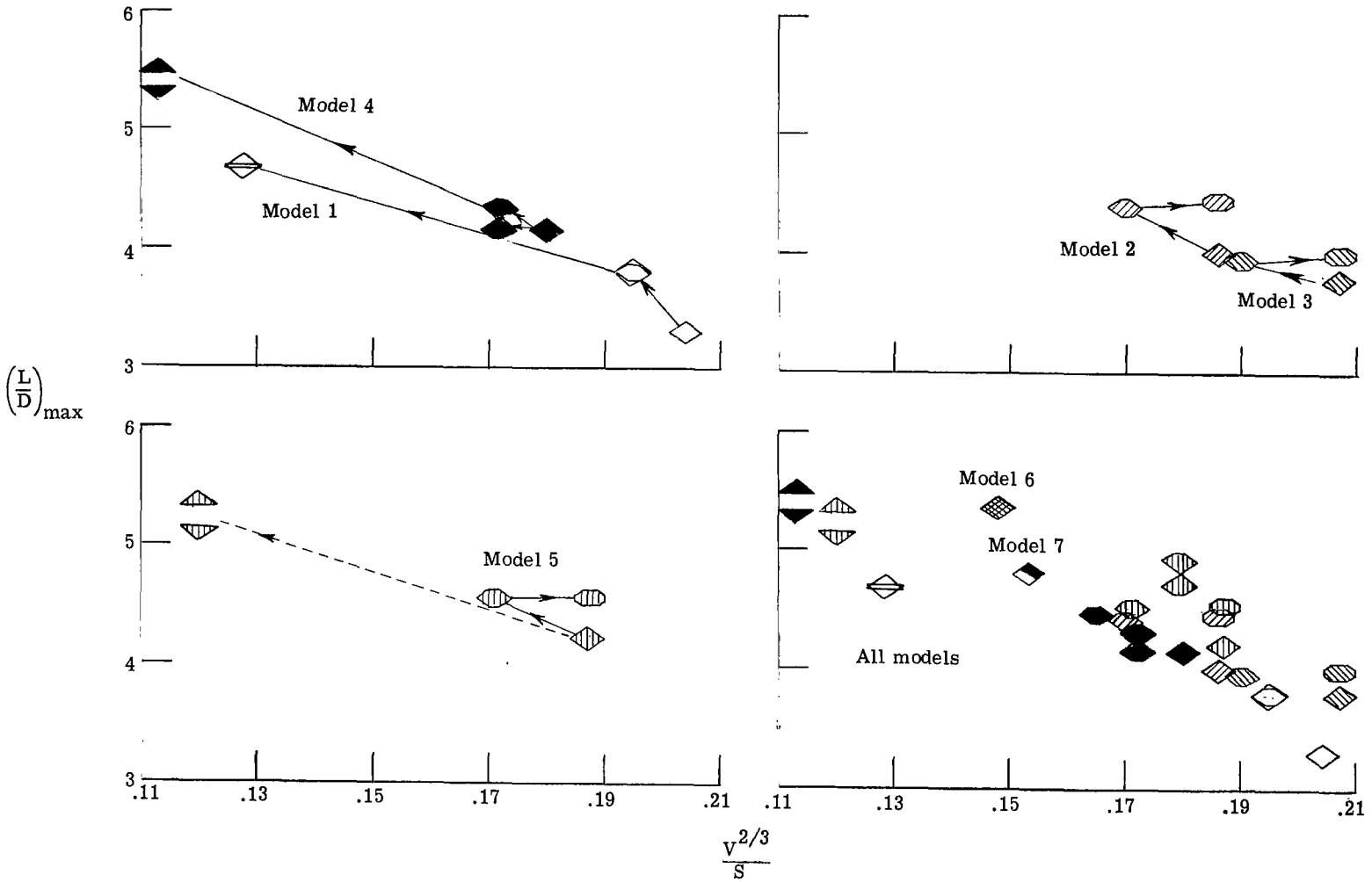

Figure 4.- Effects of modifications on $(L/D)_{max}$. $M_\infty = 6.8$; $R_{\infty,c_r} = 1.4 \times 10^6$. (Models are differentiated by shading and also by the model number; arrows show the sequence of modification; symbol shape represents the cross section of the base.)

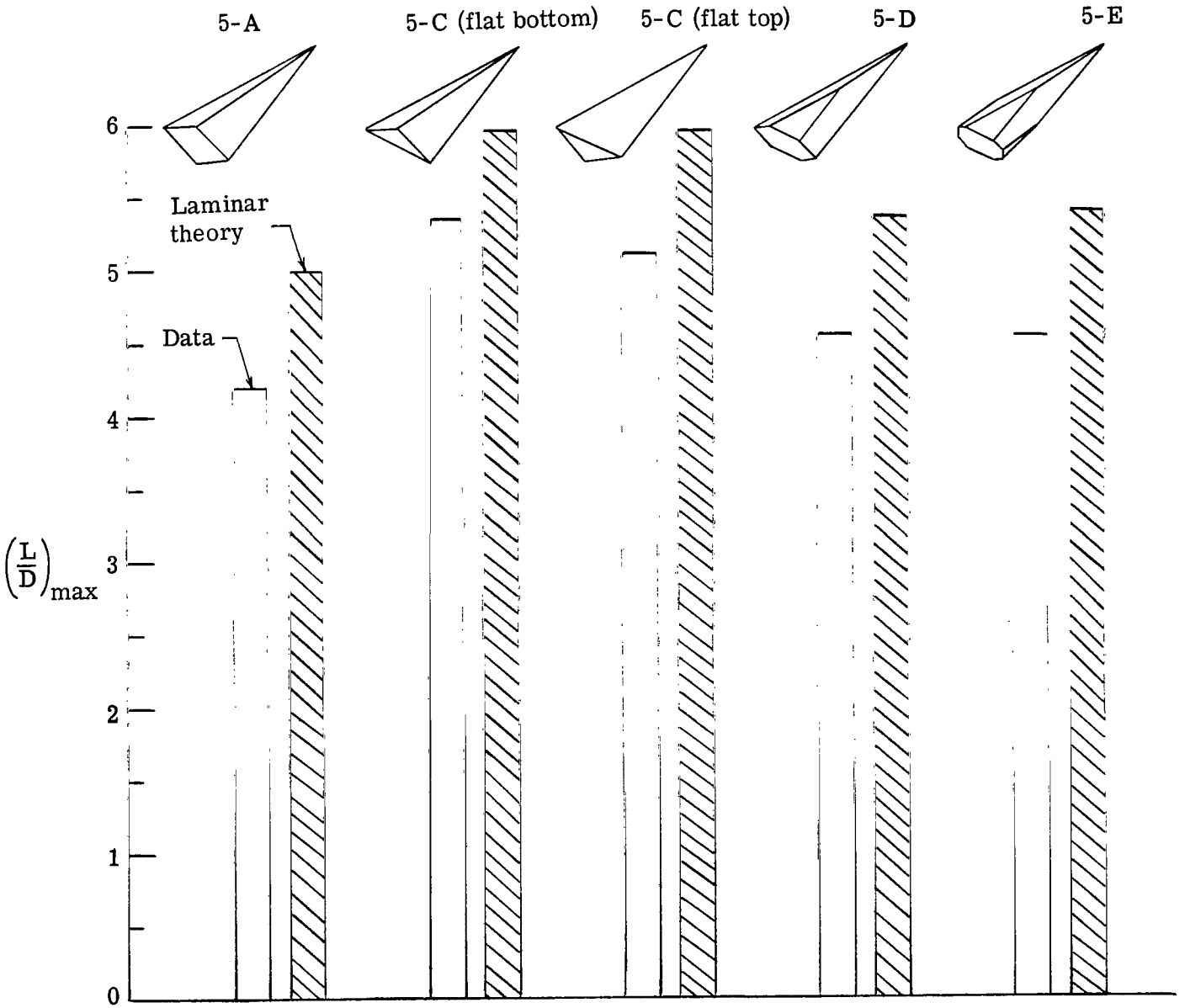

Figure 5.- Comparison between laminar theory and experimental data for aerodynamic efficiencies for various modifications to a typical model (model 5). $M_\infty = 6.8$; $R_{\infty,c_r} = 1.4 \times 10^6$.

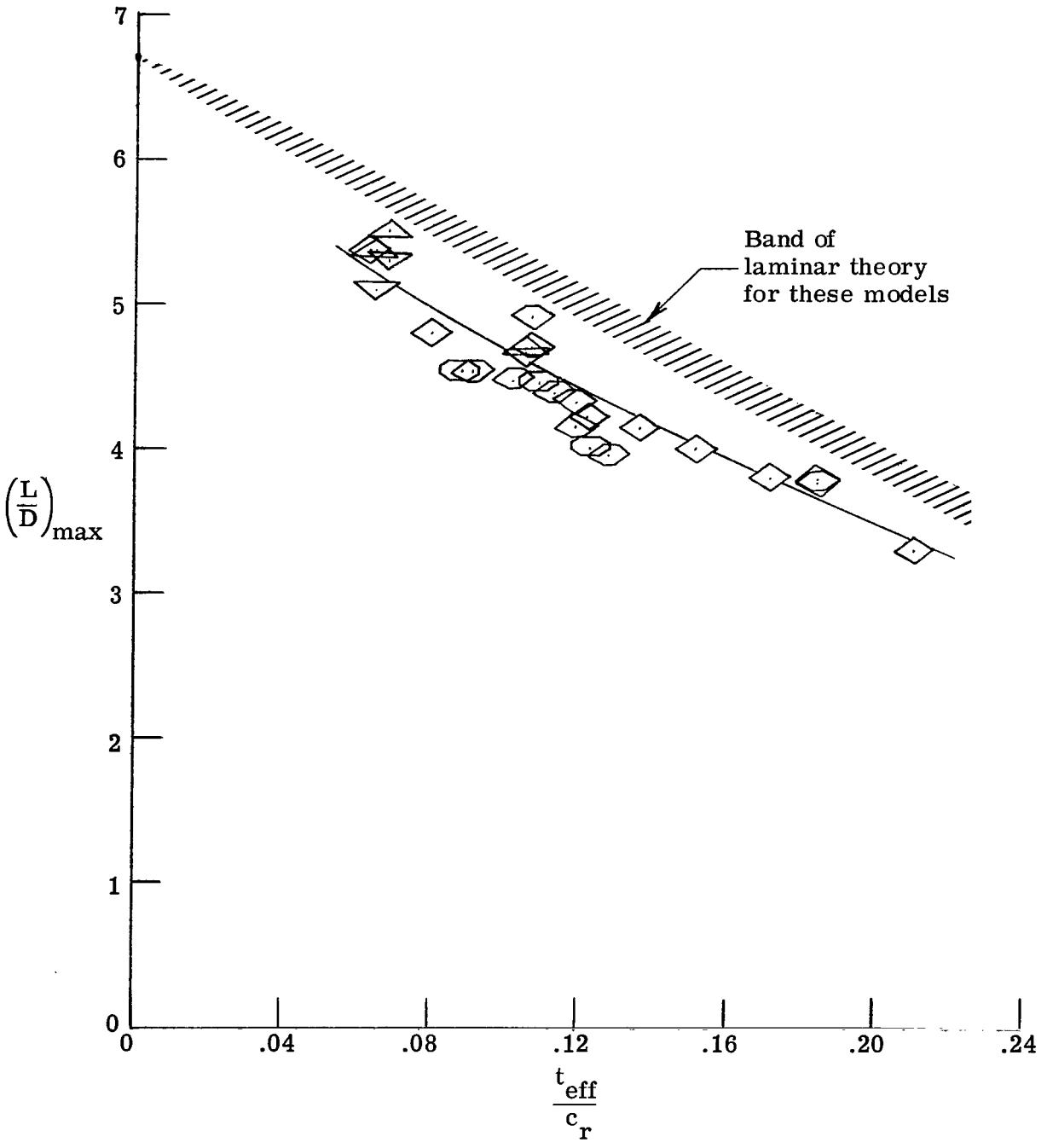

Figure 6.- Correlation of $(L/D)_{max}$ by the use of an effective thickness ratio. $M_\infty = 6.8$; $R_{\infty,c_r} = 1.4 \times 10^6$.

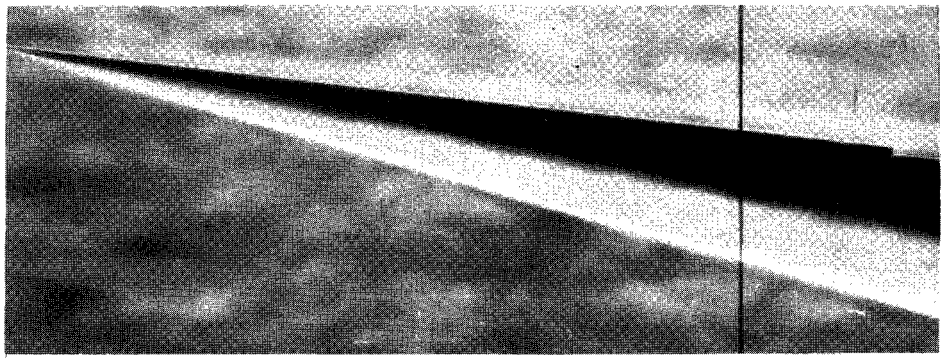

(a) Model 4-C; flat bottom; $\alpha = 10^{0}$.

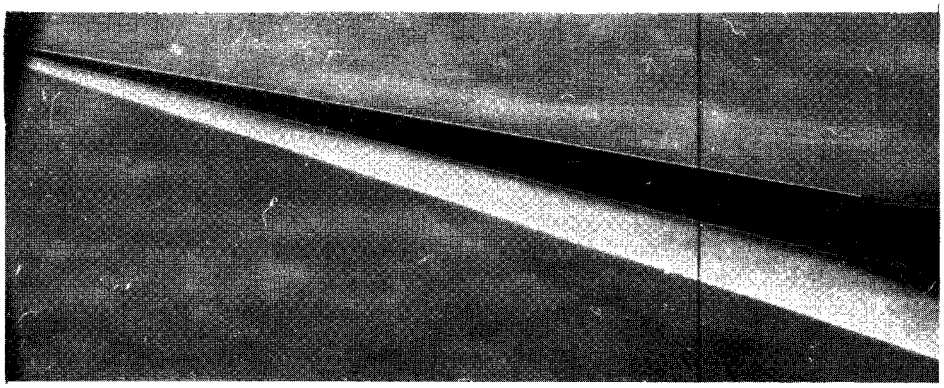

(b) Model 5-C; flat top; $\alpha = 10^{0}$.

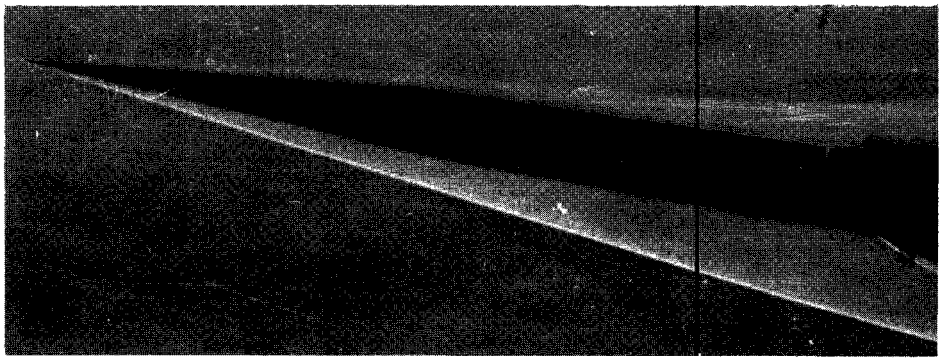

(c) Model 2-D; $\alpha = 6^{0}$. L-66-7636

Figure 7.- Side-view schlieren photographs of three modified delta wings at fairly high angles of attack. $M_{\infty} = 6.8$; $R_{\infty,c_r} = 1.4 \times 10^{6}$.

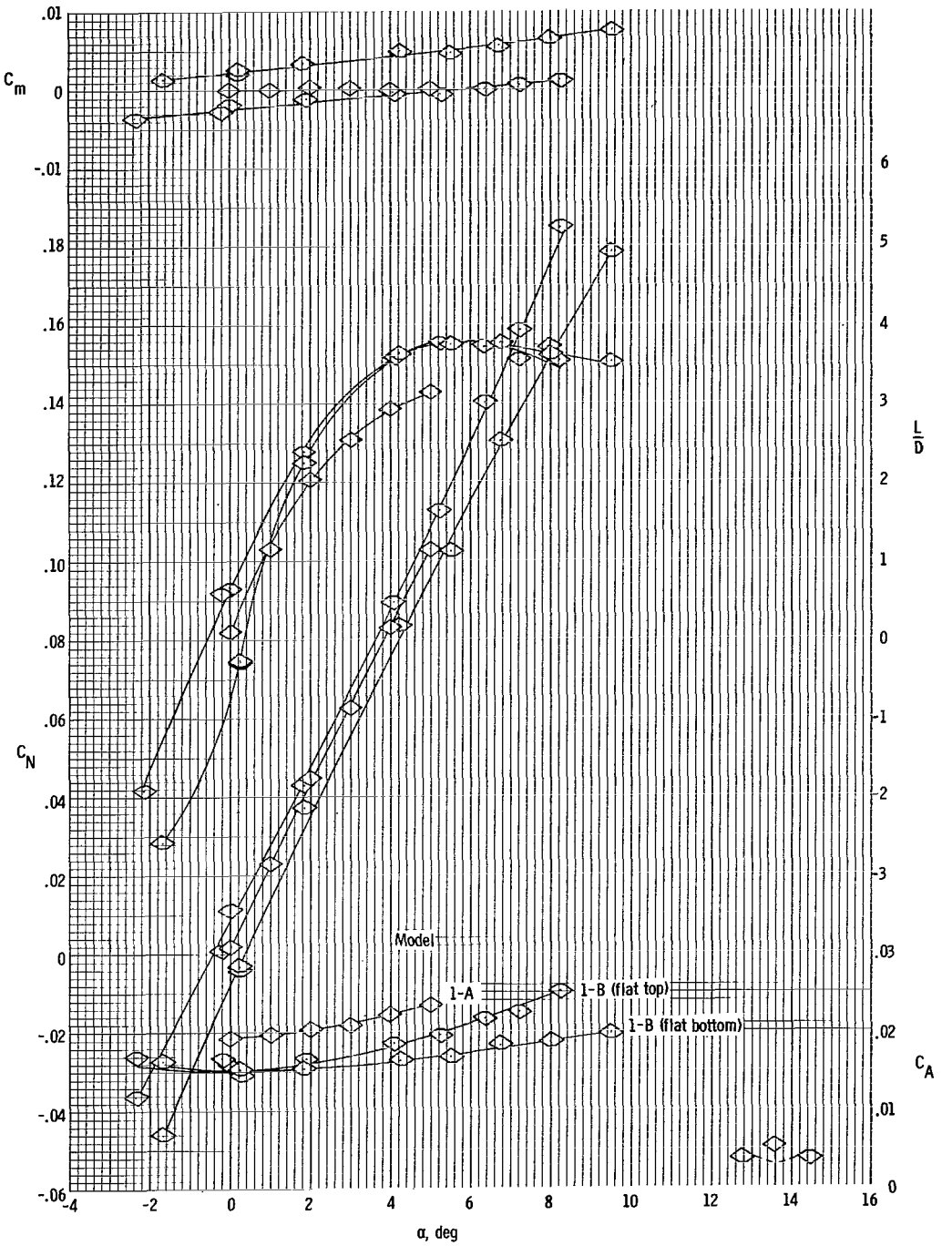

(a) Models 1-A and 1-B.

Figure 8.- Basic aerodynamic data for various models. $M_\infty = 6.8$; $R_{\infty,c_r} = 1.4 \times 10^6$. (Tick mark on α scale denotes α for shock detachment.)

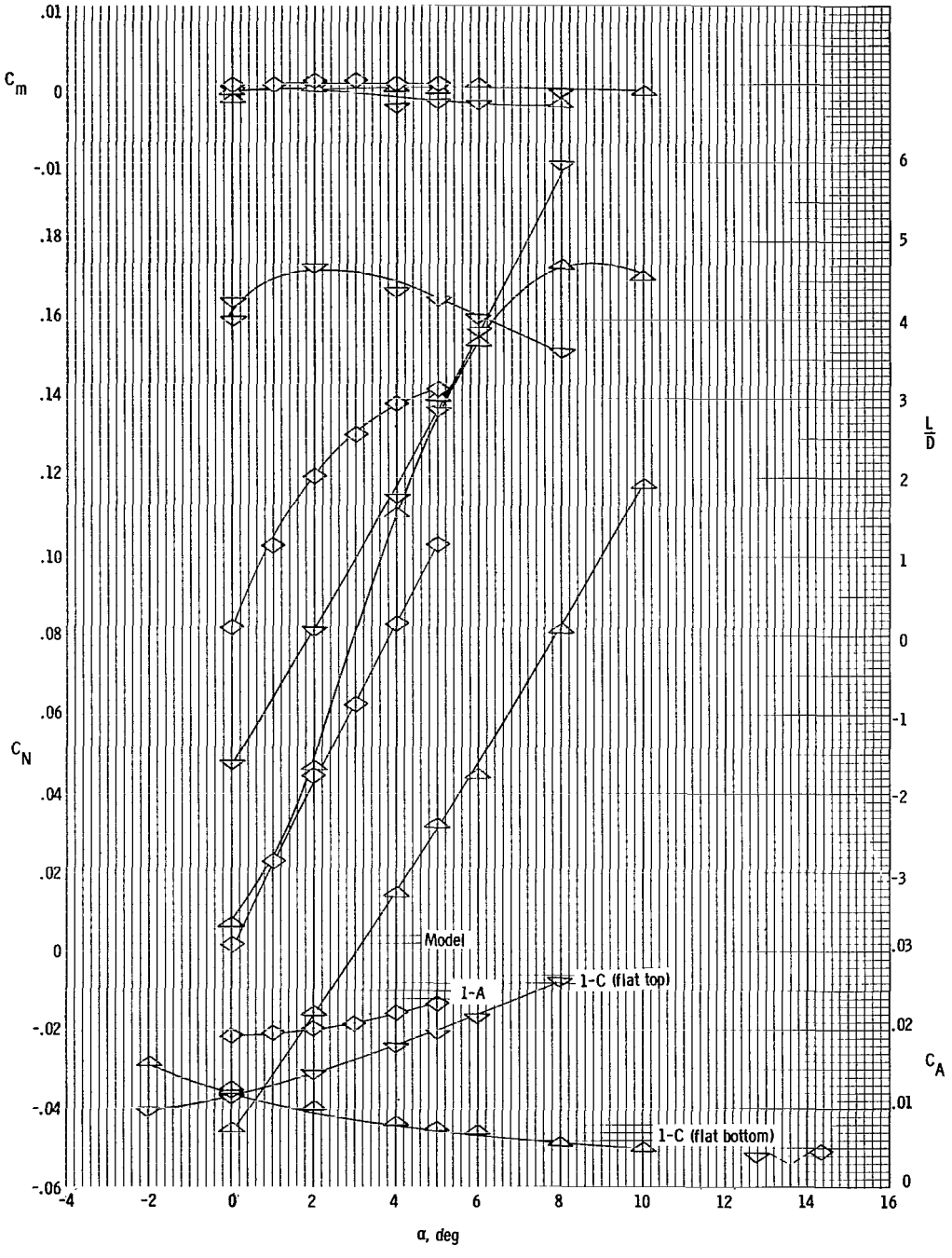

(b) Models 1-A and 1-C.

Figure 8.- Continued.

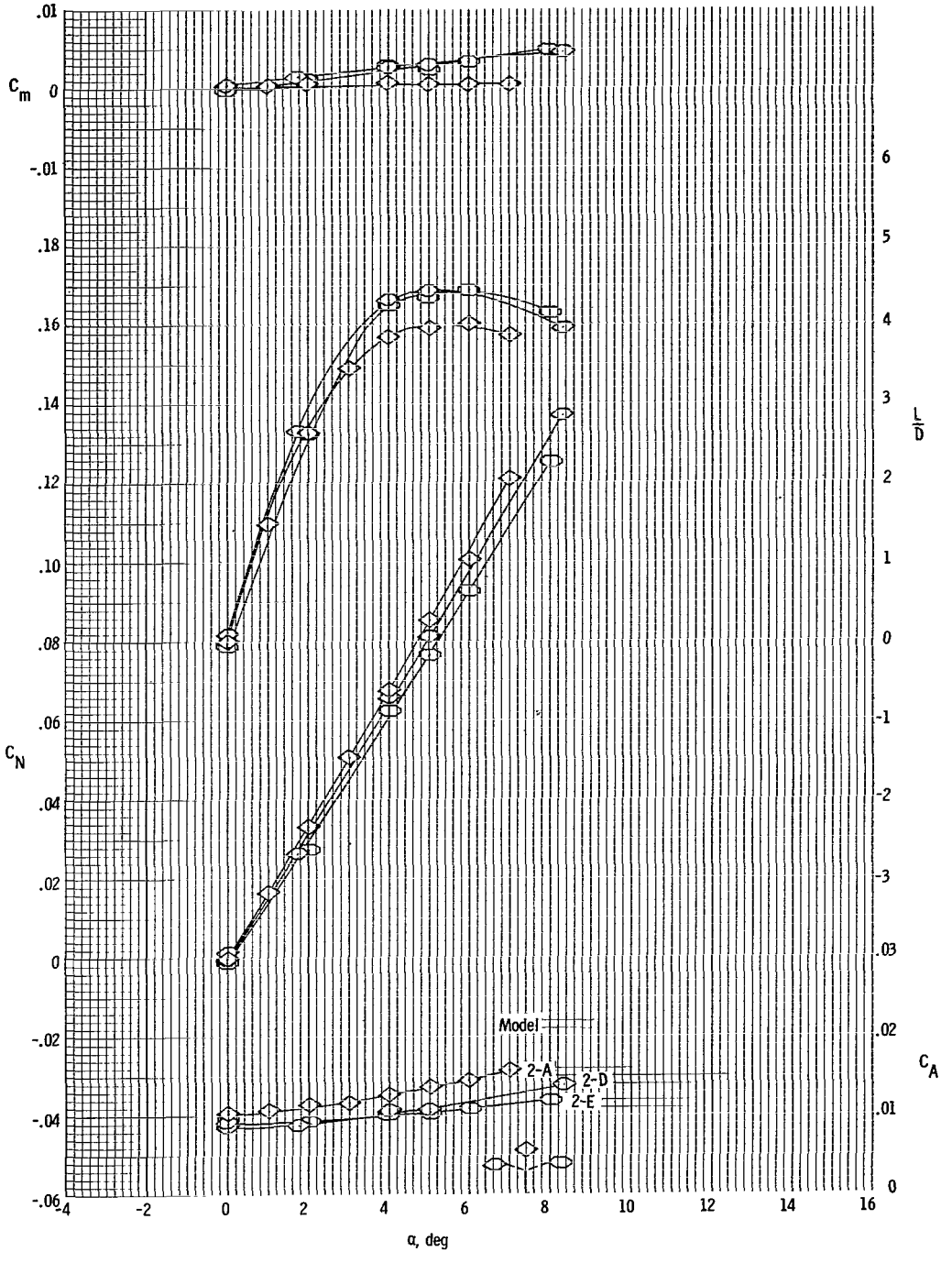

(c) Models 2-A, 2-D, and 2-E.

Figure 8.- Continued.

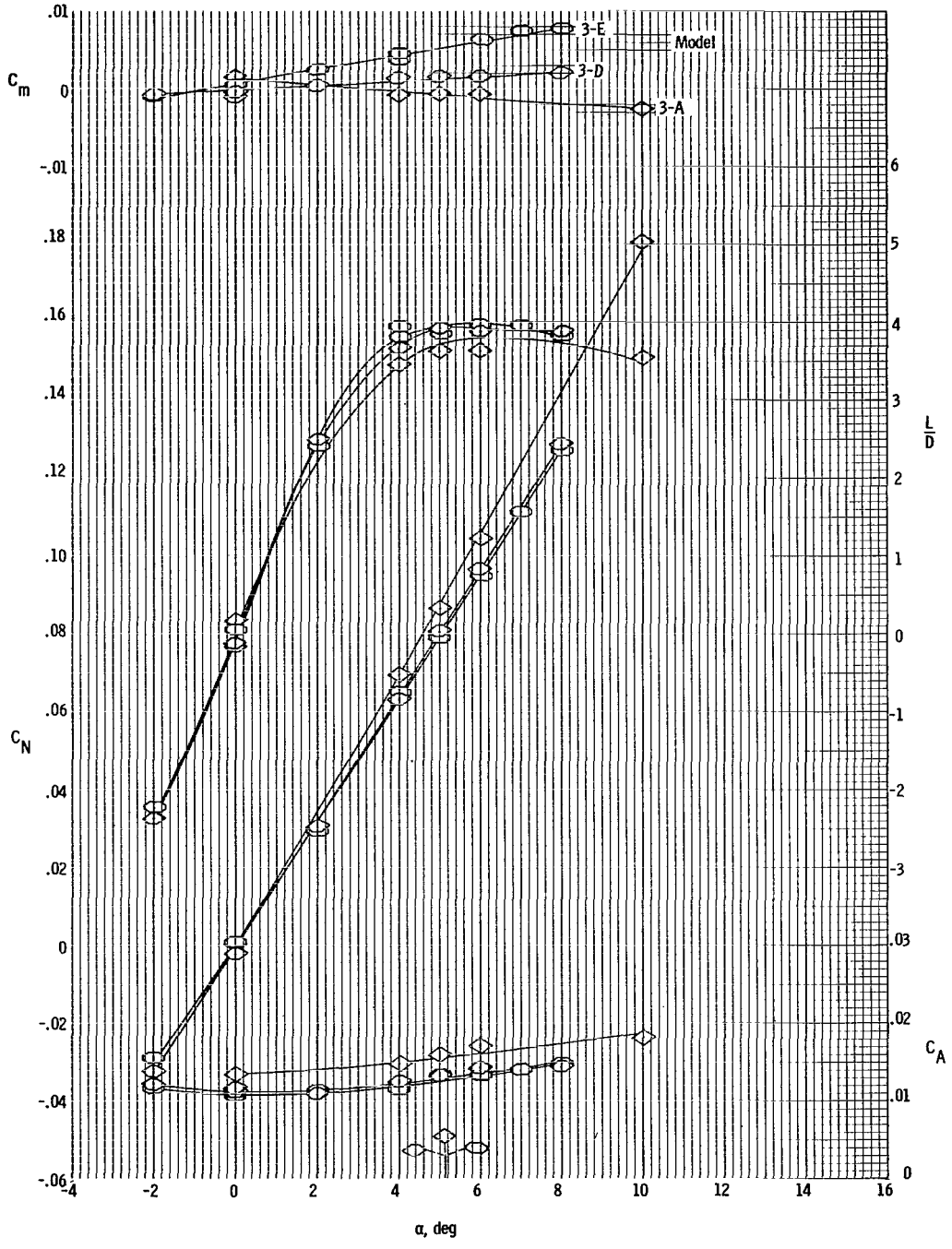

(d) Models 3-A, 3-D, and 3-E.

Figure 8.- Continued.

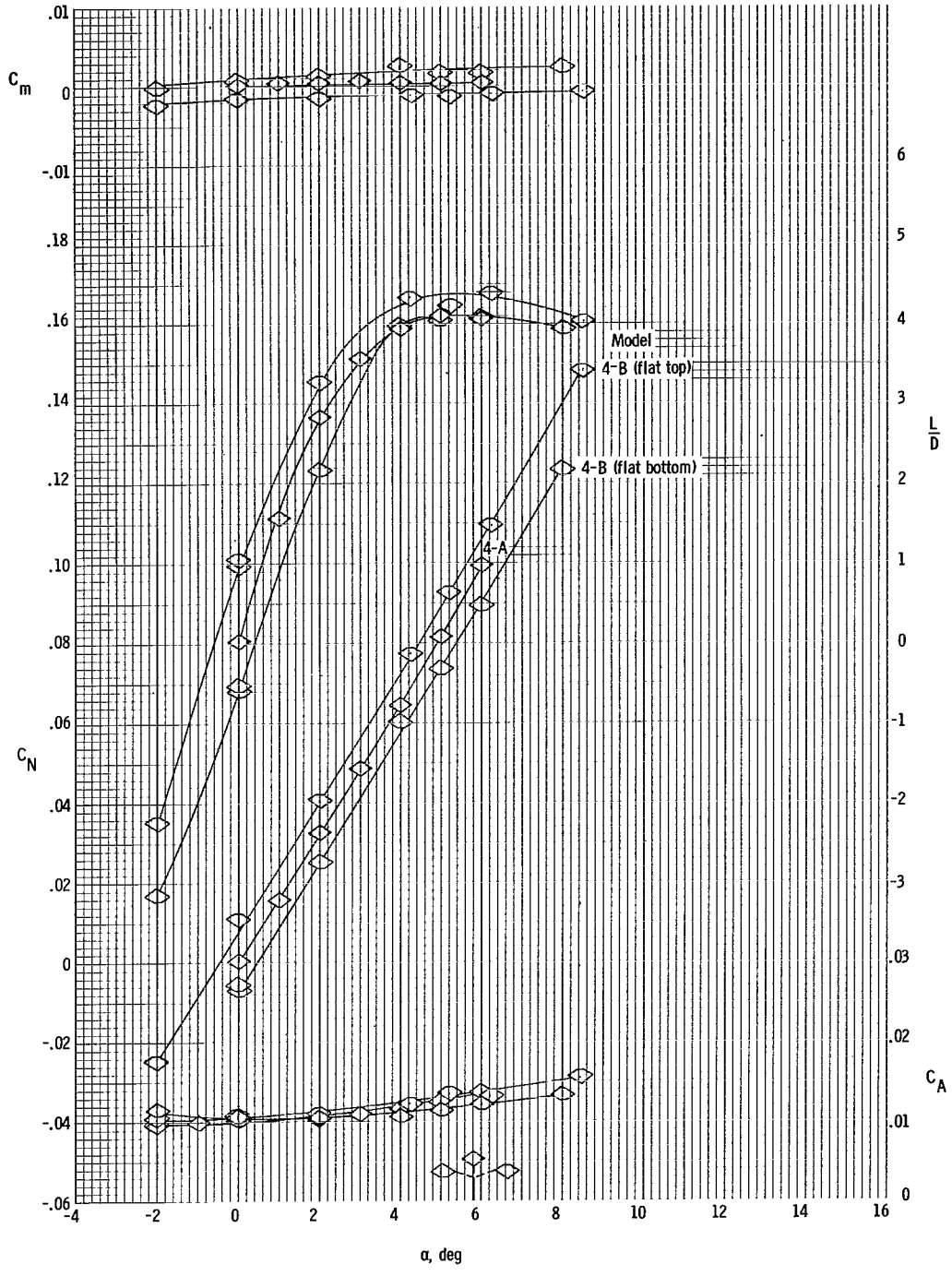

(e) Models 4-A and 4-B.

Figure 8.- Continued.

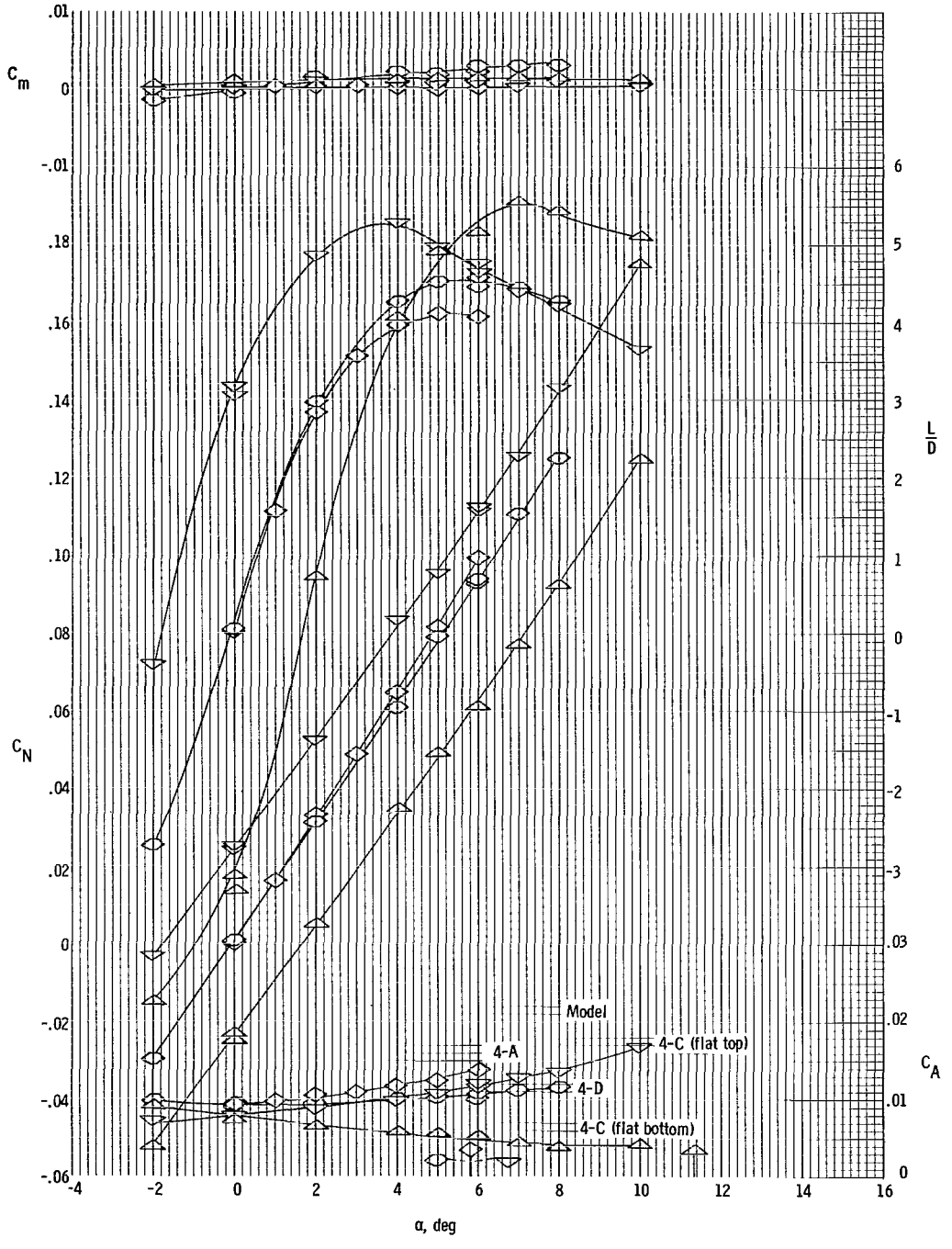

(f) Models 4-A, 4-C, and 4-D.

Figure 8.- Continued.

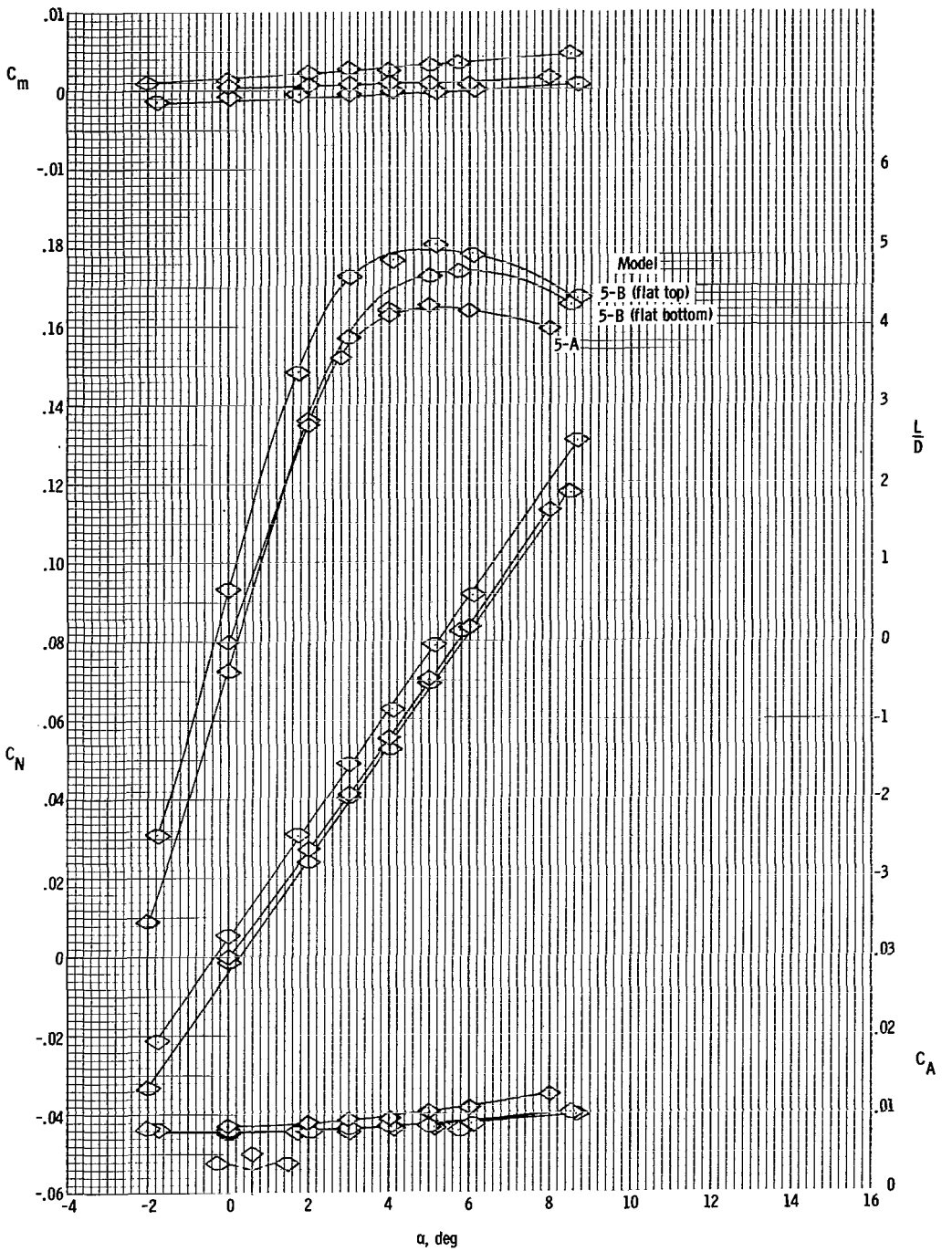

(g) Models 5-A and 5-B.

Figure 8.- Continued.

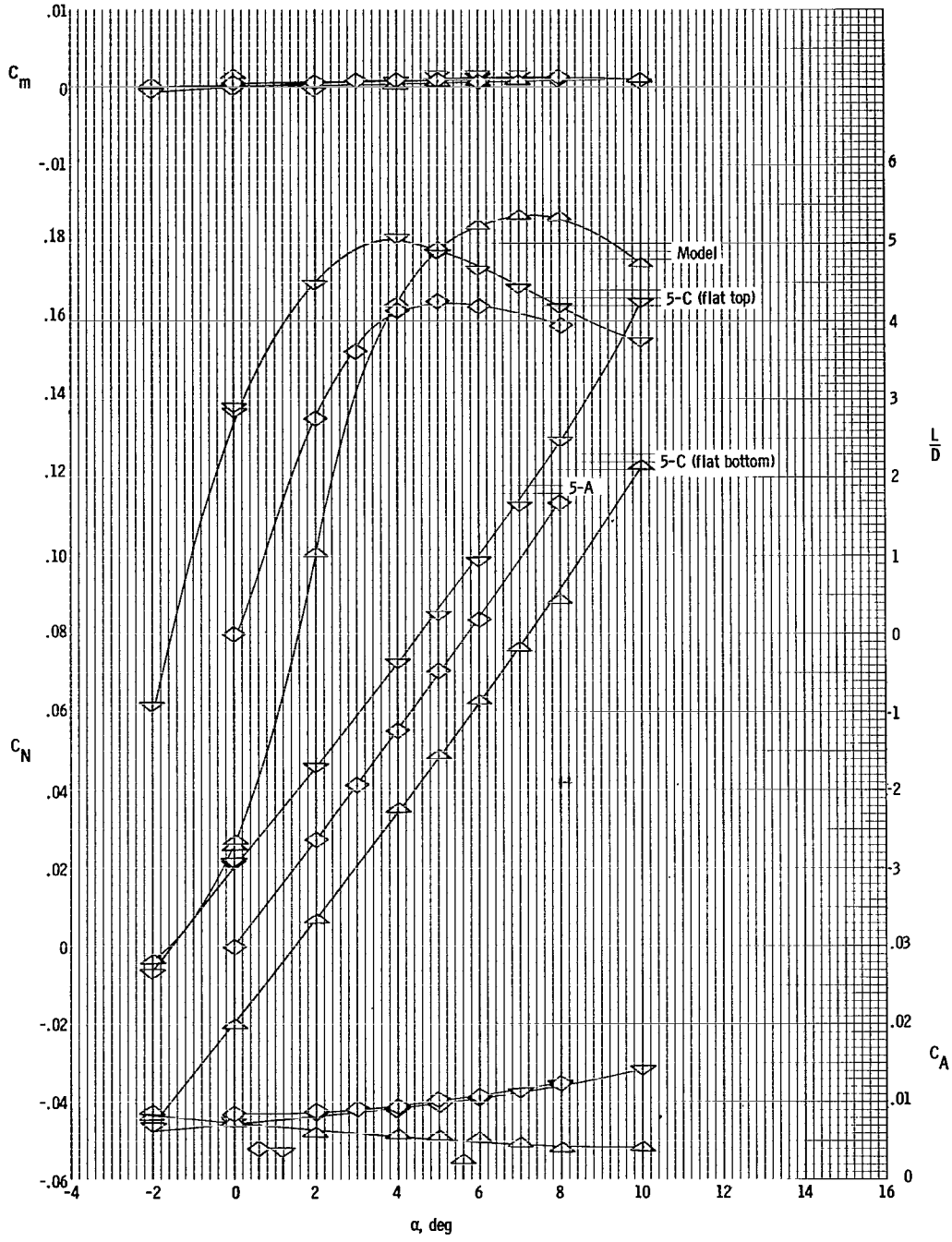

(h) Models 5-A and 5-C.

Figure 8.- Continued.

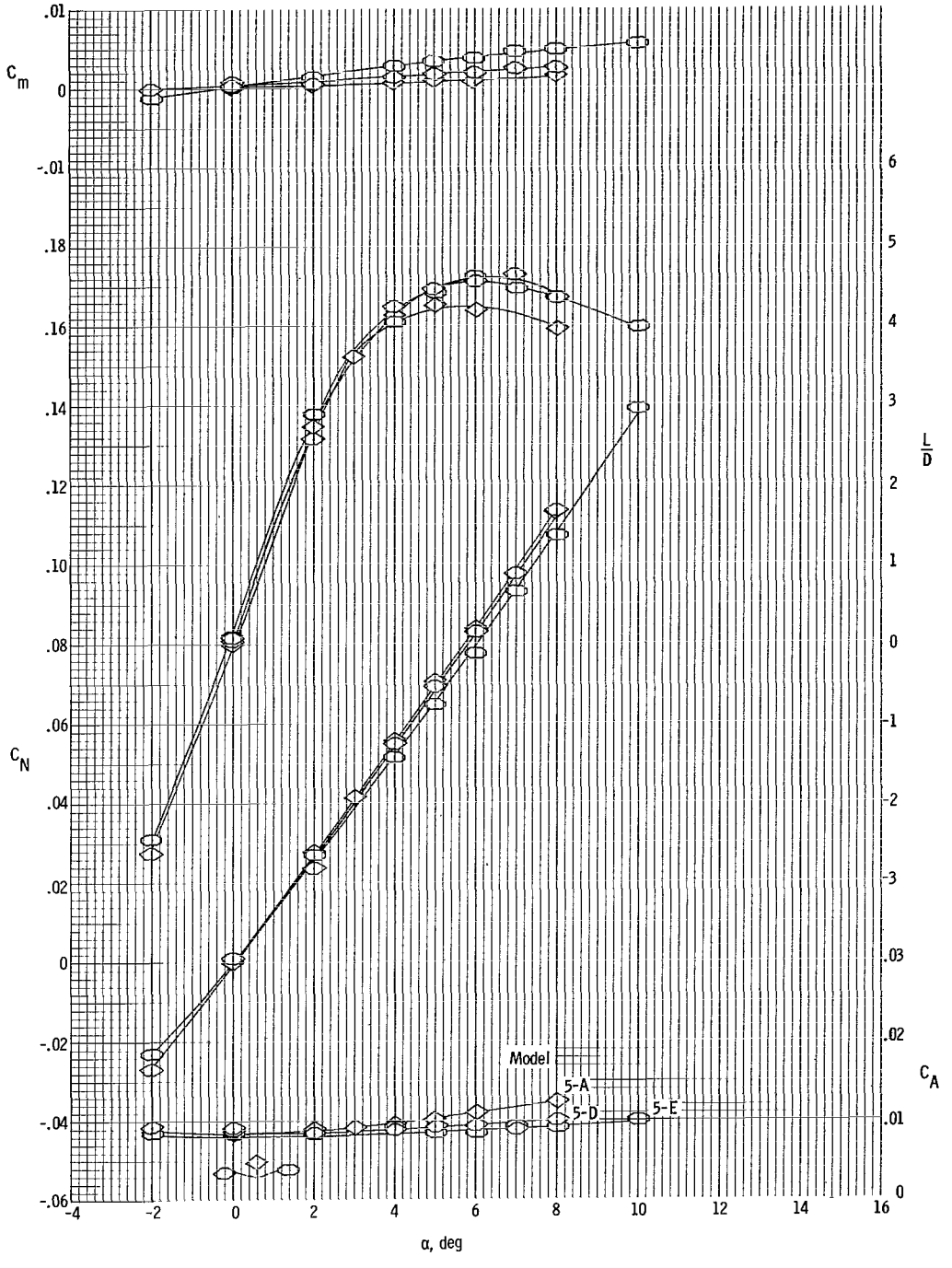

(i) Models 5-A, 5-D, and 5-E.

Figure 8.- Continued.

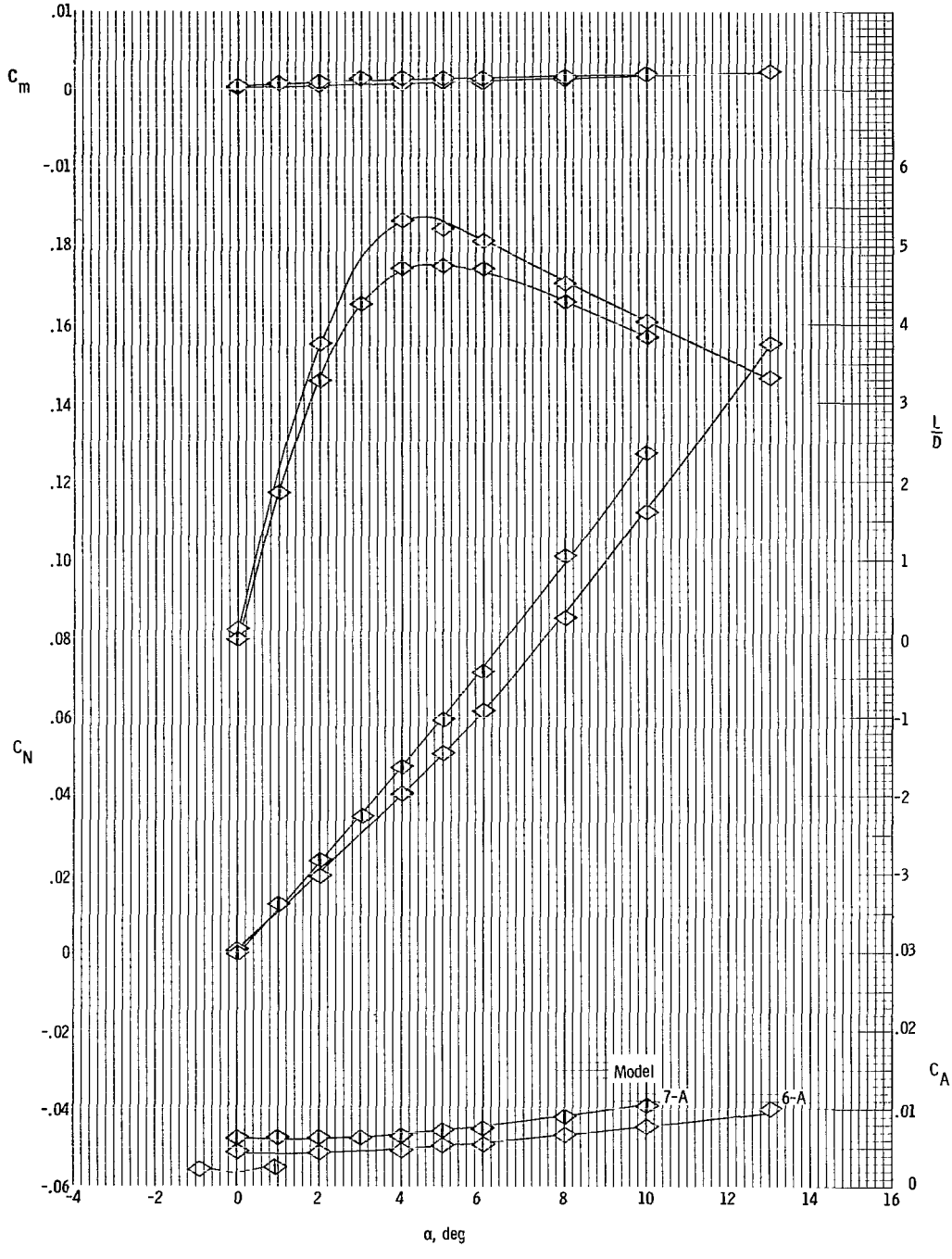

(j) Models 6-A and 7-A.

Figure 8.- Concluded.

"The aeronautical and space activities of the United States shall be conducted so as to contribute . . . to the expansion of human knowledge of phenomena in the atmosphere and space. The Administration shall provide for the widest practicable and appropriate dissemination of information concerning its activities and the results thereof."

—NATIONAL AERONAUTICS AND SPACE ACT OF 1958

NASA SCIENTIFIC AND TECHNICAL PUBLICATIONS

TECHNICAL REPORTS: Scientific and technical information considered important, complete, and a lasting contribution to existing knowledge.

TECHNICAL NOTES: Information less broad in scope but nevertheless of importance as a contribution to existing knowledge.

TECHNICAL MEMORANDUMS: Information receiving limited distribution because of preliminary data, security classification, or other reasons.

CONTRACTOR REPORTS: Scientific and technical information generated under a NASA contract or grant and considered an important contribution to existing knowledge.

TECHNICAL TRANSLATIONS: Information published in a foreign language considered to merit NASA distribution in English.

SPECIAL PUBLICATIONS: Information derived from or of value to NASA activities. Publications include conference proceedings, monographs, data compilations, handbooks, sourcebooks, and special bibliographies.

TECHNOLOGY UTILIZATION PUBLICATIONS: Information on technology used by NASA that may be of particular interest in commercial and other non-aerospace applications. Publications include Tech Briefs, Technology Utilization Reports and Notes, and Technology Surveys.

Details on the availability of these publications may be obtained from:

SCIENTIFIC AND TECHNICAL INFORMATION DIVISION

NATIONAL AERONAUTICS AND SPACE ADMINISTRATION

Washington, D.C. 20546